JOURNAL OF CATALYSIS 102, 216–233 (1986)

Acidic Properties of Binary Oxide Catalysts

II. Mössbauer Spectroscopy and Pyridine Adsorption for Iron Supported on Magnesia, Alumina, and Titania

GLEN CONNELL[1] AND J. A. DUMESIC[2]

Department of Chemical Engineering, University of Wisconsin, Madison, Wisconsin 53706

Received February 6, 1986; revised July 1, 1986

The acidic properties of MgO, Al_2O_3, and TiO_2 were studied using pyridine adsorption. Infrared spectroscopy and gravimetric adsorption measurements indicate no acid sites on MgO, while Lewis acid sites were observed on the surfaces of Al_2O_3 and TiO_2. Doping Fe onto MgO and Al_2O_3 was shown by Mössbauer spectroscopy to produce only highly coordinated Fe (e.g., sixfold coordination). A small amount of low coordination iron (e.g., fourfold coordination) was observed on TiO_2. Pyridine adsorption measurements showed that addition of Fe on MgO did not generate acidity, whereas iron produced a small number of sites on Al_2O_3 and iron addition caused a selective poisoning and strengthening of the acid sites on TiO_2. All acids in this series of single component and binary component oxides were Lewis acids. A model of Lewis acidity is proposed in that the existence of coordinatively unsaturated cations responsible for the acidic properties can be predicted using Pauling's electrostatic bond strength rules. This model is also shown to be valid for iron cations deposited on SiO_2.

INTRODUCTION

The acidic properties of metal oxides are generally thought to play an important role in determining the adsorptive and catalytic properties of these materials. Moreover, it has been found that the acidic properties of mixed metal oxides are particularly important, since the number, strength, and nature of the acid sites can be controlled by varying the composition and treatment of the sample (e.g., (*1–3*)). The materials used in most previous studies have been prepared over wide composition ranges by coprecipitation procedures. While these mixed oxides display unique acidic properties, they have complex structures; and, this has made it difficult to relate the observed acidic properties to the structure of the catalyst.

The present study was undertaken to probe the possible relationships between acidic and structural properties for a series of model mixed oxide samples prepared by depositing one metal oxide at low loadings on the surface of a second, supporting metal oxide. In the first paper of this series (*4*) it was shown that Lewis acid sites were generated by depositing iron cations on silica. The present paper addresses the acidic properties of iron supported on MgO, Al_2O_3, and TiO_2. As in our previous paper, pyridine adsorption will be used to probe the acid sites on these supported iron samples, as studied by gravimetric adsorption measurements and infrared spectroscopy. The state of iron in these samples will be monitored by Mössbauer spectroscopy.

The most general conceptual model currently available to predict the acidity generated by mixing two metal oxides is that of Tanabe *et al.* (*5*). This model is based on certain assumptions about the structure of the mixed oxide, e.g., the coordination of the oxygen anions is dictated by the structure of that oxide component present in greater concentration. In addition, this

[1] Present address: 3M Center, St. Paul, MN 55144.

[2] To whom correspondence should be addressed.

0021-9517/86 $3.00

model attempts to predict the acid type (Lewis versus Brønsted) based on electrical charge balances. The samples of the present study were chosen to test the predictions of the Tanabe model for supported metal oxides. This is possible since the structure of the acid sites associated with iron cations can be determined by Mössbauer spectroscopy and the number and type of the acid sites can be determined by gravimetric and infrared spectroscopic studies of pyridine adsorption. It will be shown that the essential assumptions of the Tanabe model appear to be correct; however, this model cannot be used to predict the type of acid sites formed by depositing one oxide onto a supporting oxide. Instead, it will be shown that a simple model based on Pauling's electrostatic bond strength (*6*) is effective in predicting the appearance and type of the acid sites. Finally, this model will be tested further in a subsequent paper in which the acidic properties of a series of metal oxides supported on silica at low loadings will be studied (*7*).

EXPERIMENTAL

Sample preparation. All supported iron oxide samples were prepared by incipient wetness impregnation of the appropriate support using 0.5 ml of an aqueous solution of ferric nitrate per gram of support. Samples for Mössbauer spectroscopy were prepared using iron enriched to about 90% with ^{57}Fe. The $^{57}Fe(NO_3)_3$ required for these syntheses was made by reduction of $^{57}Fe_2O_3$ in H_2 at 723 K overnight, followed by dissolution of the resulting metallic iron in 30 wt% HNO_3. The acid solution was allowed to evaporate at room temperature, and the iron nitrate crystals were then dissolved in water to form the impregnation solutions. The various supports used in this work are described below.

Magnesium oxide was made by precipitating $Mg(NO_3)_2$ (Aldrich 99.999%) with NH_4OH (Baker Ultrex) to form $Mg(OH)_2$. This was decomposed in vacuum while heating to 1273 K (*8*), followed by oxidation in O_2 for 72 h at 973 K. After this procedure, X-ray diffraction peaks due only to MgO were observed. This procedure produced MgO with a surface area of 61 m^2/g measured volumetrically using the BET method with nitrogen at 77 K. The Fe/MgO sample was then made to a loading of 0.8 wt% Fe using incipient wetness impregnation. Finally, the sample was heated in air at 400 K overnight.

The γ-Al_2O_3 used in this work was obtained in high purity (99.99%) from American Cyanamid. It was pretreated by oxidation in O_2 at 773 K. The surface area was determined to be 172 m^2/g using the BET method. An α-Al_2O_3 support was made by treatment of the γ-Al_2O_3 in O_2 at 1423 K for 24 h (*9*). X-Ray diffraction of the sample showed only peaks indicative of α-Al_2O_3. However, because of the random distribution of the Al cations in the tetrahedral and octahedral sites of γ-Al_2O_3, only a very broad diffraction pattern is observed even for 100% γ-Al_2O_3. Hence, the absence of the broad peaks for γ-Al_2O_3 is not indicative of the absence of tetrahedral Al cations, especially at the surface. The surface area of the α-Al_2O_3 was 14.3 m^2/g. Samples for Mössbauer spectroscopy were made by incipient wetness impregnation to a loading of 0.2 wt% Fe on γ-Al_2O_3. Gravimetric adsorption measurements and infrared spectroscopy were carried out on samples with a loading of 0.6 wt% Fe.

The titania used in this work was Degussa P-25. It was cleaned as described by Santos *et al.* (*10*). In short, the TiO_2 was washed with H_2O to remove foreign ions and oxidized in O_2 at 700 K to remove residual hydrocarbons. The titania had a surface area of 54 m^2/g. The iron-containing samples for all studies were made with loadings of 0.6 wt% Fe using incipient wetness impregnation.

Acidity measurements and Mössbauer spectroscopy. The acidic properties of the samples were measured using pyridine adsorption. The amount of adsorbed pyridine following exposure to 4.8 Torr (1 Torr =

133.3 Pa) of pyridine and evacuation at progressively higher temperatures was determined gravimetrically using a quartz-spring balance, as described in Part I of this series (*4*). Prior to these measurements, the samples of iron supported on MgO, Al_2O_3, and TiO_2 were treated in O_2 at 723 K. In some cases, one subsequent treatment was employed, that being reduction in H_2 at 723 K. The type of acid sites on the various samples was determined using infrared spectroscopy of adsorbed pyridine. This procedure has also been described in detail in Part I of this series (*4*). In short, the samples were exposed to 4.8 Torr of pyridine at 423 K followed by evacuation at this and progressively higher temperatures.

In situ Mössbauer spectra were collected at room temperature following various treatments of the supported iron samples in O_2 and in H_2 at elevated temperatures. The velocity scale in all spectra is reported relative to metallic iron at room temperature. There was an Fe impurity in the Be windows used on the *in situ* Mössbauer spectroscopy cell. The spectrum for this impurity has been numerically subtracted from the shown spectra. This procedure as well as the computer fitting methods used to analyze the Mössbauer spectra are described elsewhere (*4*).

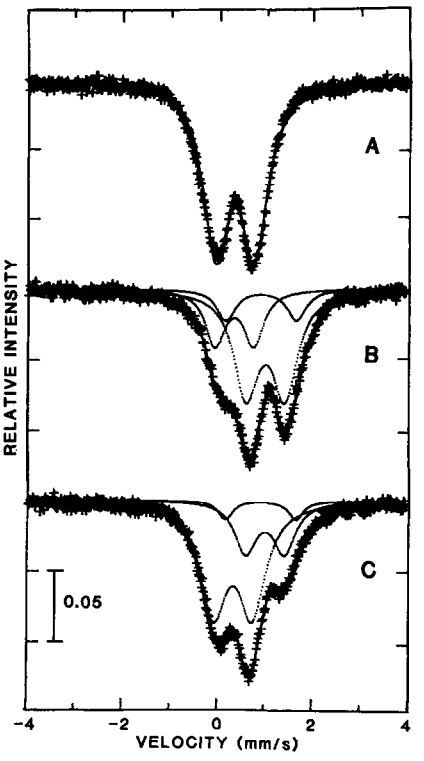

FIG. 1. Room temperature Mössbauer spectra for 0.8 wt% Fe/MgO. (A) After oxidation in O_2 at 723 K; (B) after reduction in H_2 at 723 K; (C) after oxidation in O_2 at 295 K.

RESULTS

Iron Supported on MgO

Mössbauer spectroscopy. Mössbauer spectra of the Fe/MgO sample are shown in Fig. 1. Spectrum A is after treatment in O_2 at 723 K for 4 h. The spectrum has been fit with a doublet having an isomer shift of 0.33 mm/s and a quadrupole splitting of 0.82 mm/s. All the fitting parameters are listed in Table 1. The fit using the one doublet is not exact since there is probably a distribution of sites on the surface, but the spectrum does not lend itself to more refined fitting.

Reduction of the sample at 723 K in H_2 for 4 h leads to the formation of Fe^{2+} as seen in Fig. 1B. This spectrum has been fit with three doublets. The left-most doublet is that of Fe^{3+}, and the isomer shift and quadrupole splitting of this doublet have been constrained to be the same as for the oxidized sample. Two new doublets for Fe^{2+} have been used to fit the spectrum. The one with the larger area has an isomer shift of 0.99 mm/s and a quadrupole splitting of 0.82 mm/s. This doublet has been assigned to Fe^{2+} cations in the bulk of MgO as a substitutional solid (*11*, *12*). The other doublet has an isomer shift of 0.90 mm/s and a quadrupole splitting of 1.5 mm/s. These parameters are indicative of high coordination iron, e.g., five- or sixfold coordination. The large amount of Fe^{3+} that remains after reduction is indicative of the formation of magnesium ferrite, $MgFe_2O_4$. Formation of this bulk phase renders the Fe^{3+} inaccessible to gas phase reduction.

TABLE 1

Mössbauer Parameters for Spectra of 0.8 wt% Fe/MgO Shown in Fig. 1

Species		Treatment: gas and temperature		
		O_2 723 K	H_2 723 K	O_2 295 K
Fe^{3+}				
Isomer shift	0.33 mm/s			
Quadrupole splitting	0.82 mm/s			
Fractional area		1.00	0.25	0.67
Linewidth (mm/s)		0.67	0.50	0.67
Area (pct. * mm/s)		24.41	6.01	16.02
Fe^{2+} inner doublet				
Isomer shift	0.99 mm/s			
Quadrupole splitting	0.82 mm/s			
Fractional area			0.60	0.26
Linewidth (mm/s)			0.64	0.56
Area (pct. * mm/s)			14.24	6.23
Fe^{2+} outer doublet				
Isomer shift	0.90 mm/s			
Quadrupole splitting	1.49 mm/s			
Fractional area			0.14	0.07
Linewidth (mm/s)			0.49	0.37
Area (pct. * mm/s)			3.39	1.59

Since the major Fe doublets can be assigned to Fe^{2+} cations in MgO and Fe^{3+} cations in $MgFe_2O_4$, it is questionable as to how much Fe remains on the surface of MgO. Oxidation of the sample at room temperature for 4 h leads to the spectrum shown in Fig. 1C. As can be seen, the amount of Fe^{3+} increases and the amount of Fe^{2+} decreases, but a large amount of the iron is not affected by the oxidation. Room temperature oxidation oxidizes 40% of the Fe from Fe^{2+} to Fe^{3+}. This indicates that 60% of the Fe is in the bulk and is not affected by the reduction or oxidation. Since oxidation is expected to occur through at least a few atomic layers, one can estimate that the amount of surface Fe is less than 20% of the total Fe in the sample.

Pyridine adsorption measurements. Gravimetric adsorption measurements of pyridine showed that for MgO there was less than 1×10^{-4} g of pyridine adsorbed per gram of MgO at 423 K upon evacuation to 10^{-4} Torr. Addition of Fe to the sample in both the fully oxidized and reduced states had no effect on the minimal adsorption of pyridine on MgO. Hence MgO does not contain any measurable acid sites and the addition of Fe does not alter this.

A sample of 0.8 wt% Fe/MgO evacuated at 423 K to a pyridine pressure of 9×10^{-4} Torr showed bands in the infrared region at 1442 and 1599 cm^{-1}. These peaks are shown in Fig. 2D and the frequencies are tabulated in Table 2. These bands are weak and are indicative of physisorbed pyridine. Evacuation of the sample to a lower pressure of 2×10^{-4} Torr but still at 423 K essentially removed the bands as shown in spectrum E. This is further evidence that there is only physisorbed pyridine on Fe/MgO. Evacuation at 523 K (Fig. 2F) leads to the complete loss of the pyridine spectrum.

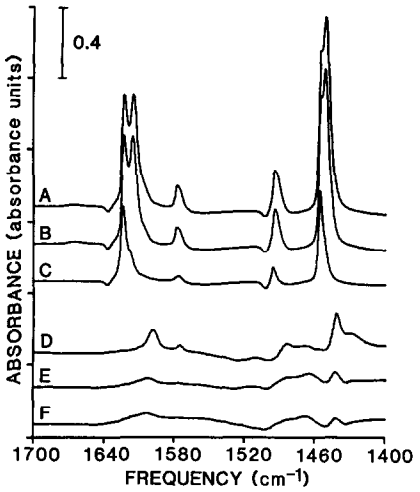

FIG. 2. Infrared spectra of pyridine adsorbed on 0.6 wt% Fe/γ-Al_2O_3 (A–C) and 0.8 wt% Fe/MgO (D–F) after oxidation in O_2 at 723 K. Evacuation temperature and pressure: (A) 423 K, 9×10^{-4} Torr; (B) 423 K, 2×10^{-4} Torr; (C) 523 K, 2×10^{-4} Torr; (D) 423 K, 9×10^{-4} Torr; (E) 423 K, 2×10^{-4} Torr; (F) 523 K, 1×10^{-4} Torr.

TABLE 2

Infrared Absorption Frequencies (cm^{-1}) for Spectra of Pyridine Adsorbed on 0.8 wt% Fe/MgO Shown in Figs. 2D–F

Type	Band	Evacuation treatment: temperature and pressure (Torr)		
		423 K, 9×10^{-4}	423 K, 2×10^{-4}	523 K, 1×10^{-4}
HPY	19b	1442	1442	
	19a	1483	1481	
	8b	1576	1576	
	8a	1599	1603	1603

Note. HPY = physisorbed or hydrogen-bonded pyridine.

Iron Supported on Al_2O_3

Mössbauer spectroscopy. Oxidation of a 0.2 wt% Fe/γ-Al_2O_3 sample in O_2 at 673 K led to the spectrum shown in Fig. 3A. This spectrum has been fit with two doublets because the breadth of the two observable peaks could not be fit with a single Lorentzian doublet. The Mössbauer parameters for the fitted spectra of Fe/Al_2O_3 are listed in Table 3. The spectrum taken after calcination at 423 K could be fit with a single doublet. However, as the oxidation temperature was increased to 473, 573, and 673 K the broadness of the peaks increased and could no longer be fit with a single doublet. This suggests that at higher temperatures the Fe is converted into a different structure on the surface. The broadness of the peaks indicates that the iron exists in a variety of sites with different symmetries. This may also be evidence for diffusion of Fe into the bulk of Al_2O_3. Since α-Fe_2O_3 and α-Al_2O_3 have the same crystal structure they have been shown to be soluble at least up to 10 at.% (*13*).

Reduction of the 0.2 wt% Fe/γ-Al_2O_3 in H_2 at 723 K yielded the spectrum shown in Fig. 3B. This spectrum has been fit with two Fe^{2+} doublets and a residual Fe^{3+} doublet whose parameters are not the same as in the oxidized sample. The two doublets for Fe^{2+} are similar to those observed for highly coordinated Fe on the surfaces of MgO and TiO_2 in the present paper and

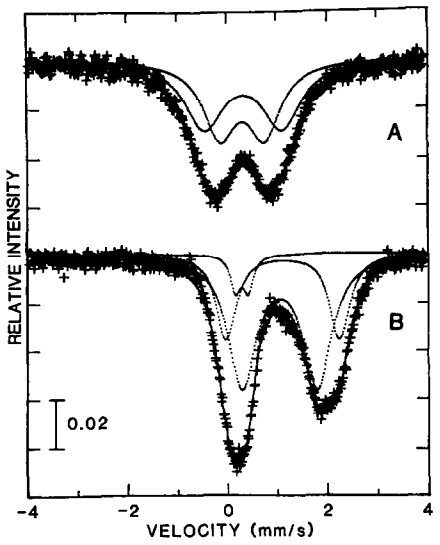

FIG. 3. Room temperature Mössbauer spectra for 0.2 wt% Fe/γ-Al_2O_3. (A) After oxidation in O_2 at 673 K; (B) after reduction in H_2 at 723 K.

TABLE 3

Mössbauer Parameters for Spectra of 0.2 wt% $Fe/\gamma\text{-}Al_2O_3$ Shown in Fig. 3

Species	Treatment: gas and temperature	
	O_2 673 K	H_2 723 K
Fe^{3+}		
Isomer shift (mm/s)	0.33/0.31	0.27
Quadrupole splitting (mm/s)	1.56/0.91	0.26
Fractional area	0.53/0.47	0.06
Linewidth (mm/s)	0.96/0.80	0.25
Area (pct. * mm/s)	8.00/7.27	1.13
Fe^{2+} outer doublet I		
Isomer shift (mm/s)		1.04
Quadrupole splitting (mm/s)		1.51
Fractional area		0.64
Linewidth (mm/s)		0.69
Area (pct. * mm/s)		11.64
Fe^{2+} outer doublet II		
Isomer shift (mm/s)		1.10
Quadrupole splitting (mm/s)		2.28
Fractional area		0.30
Linewidth (mm/s)		0.49
Area (pct. * mm/s)		5.43

SiO_2 in our previous paper (*4*). This agrees with the work of Rethwisch and Dumesic (*12*). The formation of $FeAl_2O_4$ spinel has been proposed for Fe/Al_2O_3 surfaces (e.g., (*14, 15*)). The parameters of the doublets observed in this study are similar to the parameters for $FeAl_2O_4$ which has an isomer shift of 1.08 mm/s and a quadrupole splitting of 1.60 mm/s at room temperature (*16*). Therefore, there is a strong possibility that some of this spinel has formed on the sample.

Pyridine adsorption measurements. Gravimetric measurements of pyridine adsorption showed large numbers of acid sites on the surfaces of both $\alpha\text{-}Al_2O_3$ and $\gamma\text{-}Al_2O_3$. The results for both types of Al_2O_3 after oxidation are shown in Fig. 4. It should be noted that the measurements were done with a fixed sample weight (ca. 400 mg) so that the experimental error is

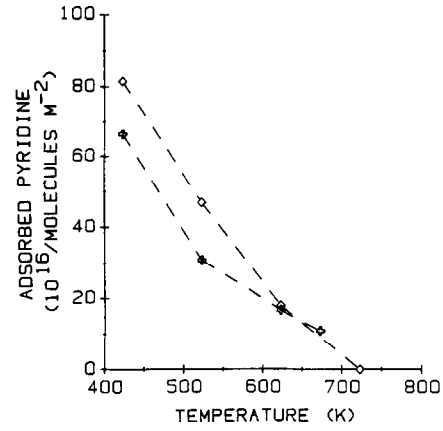

FIG. 4. Gravimetric measurements of pyridine adsorption on Al_2O_3: (◇) $\alpha\text{-}Al_2O_3$ after oxidation in O_2 at 723 K, and (✣) $\gamma\text{-}Al_2O_3$ after oxidation in O_2 at 673 K.

higher for the $\alpha\text{-}Al_2O_3$ samples than for the $\gamma\text{-}Al_2O_3$ samples because of the surface area differences.

Addition of 0.6 wt% Fe to $\gamma\text{-}Al_2O_3$ adds a small number of new acid sites on the surface. This is shown by the results of the gravimetric adsorption measurements displayed in Fig. 5. The open symbols and dashed lines are for $\gamma\text{-}Al_2O_3$ alone and the filled symbols and solid lines are for the iron-doped samples. Experiments were

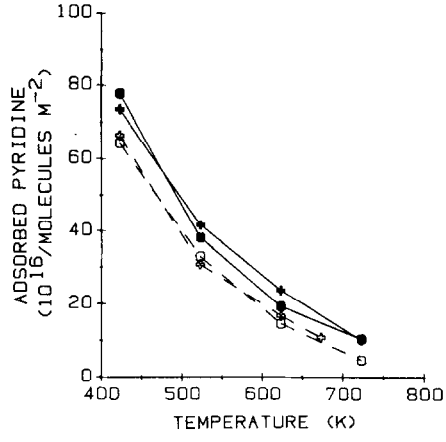

FIG. 5. Gravimetric measurements of pyridine adsorption on 0.6 wt% $Fe/\gamma\text{-}Al_2O_3$: (○) $\gamma\text{-}Al_2O_3$ after reduction in H_2 at 723 K; (✣) $\gamma\text{-}Al_2O_3$ after oxidation in O_2 at 673 K; (●) $Fe/\gamma\text{-}Al_2O_3$ after reduction in H_2 at 723 K; (✚) $Fe/\gamma\text{-}Al_2O_3$ after oxidation in O_2 at 723 K.

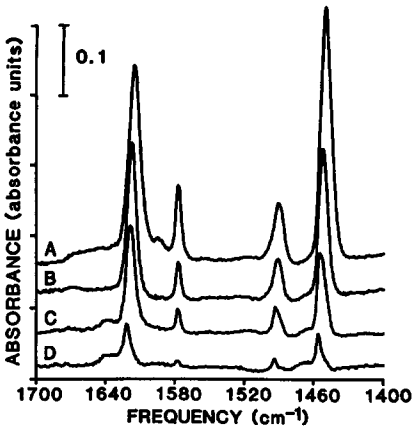

FIG. 6. Infrared spectra of pyridine adsorbed on α-Al_2O_3 after oxidation in O_2 at 723 K. Evacuation temperature and pressure: (A) 423 K, 1×10^{-3} Torr; (B) 423 K, 2×10^{-4} Torr; (C) 523 K, 2×10^{-4} Torr; (D) 623 K, 1×10^{-4} Torr.

conducted after oxidation in O_2 at 723 K and after reduction in H_2 at 723 K. As can be seen, oxidation or reduction does not affect the acidity of Al_2O_3. Addition of Fe creates new acid sites that retain the pyridine even after evacuation at 723 K. These extra sites are responsible for the increased acidity at the lower evacuation temperatures as well because the separation between the two sets of curves remains constant. The difference between the doped and undoped samples corresponds to 15% of the added Fe cations. In fact, Rethwisch and Dumesic (*17*) used nitric oxide adsorption to estimate that about 15% of the iron cations for a 1 wt% Fe/Al_2O_3 sample were on the surface. It must be noted, however, that the present gravimetric adsorption results do not unequivocally show new acid sites. The difference between the Fe/Al_2O_3 data and the Al_2O_3 data remains constant throughout the entire temperature range. Hence a possible error in the initial weights used to calculate these data would shift the curve. This shift was observed, however, for multiple runs in which the initial weights were measured independently.

The infrared spectra of pyridine adsorbed on α-Al_2O_3 are shown in Fig. 6 and the absorption frequencies are tabulated in Table 4. There is one set of Lewis acid peaks whose maxima shift upward as the evacuation is carried out at lower pressures and higher temperatures. The 8a band, for example, shifts from 1615 cm^{-1} in spectrum A to 1622 cm^{-1} in spectrum D. Evacuation at 723 K led to a spectrum with no pyridine bands.

TABLE 4

Infrared Absorption Frequencies (cm^{-1}) for Spectra of Pyridine Adsorbed on α-Al_2O_3 Shown in Fig. 6

Type	Band	Evacuation treatment: temperature and pressure (Torr)			
		423 K, 1×10^{-3}	423 K, 2×10^{-4}	523 K, 2×10^{-4}	623 K, 1×10^{-4}
LPY	19b	1449	1452	1454	1456
	19a	1490	1491	1493	1494
	8b	1577	1577	1577	
	8a	1615	1617	1618	1622
HPY	19b				
	19a				
	8b				
	8a	1600sh			

Note. LPY = Lewis pyridine; HPY = physisorbed or hydrogen-bonded pyridine; sh = shoulder.

The above behavior of α-Al_2O_3 is in contrast to the γ-Al_2O_3 spectra shown in Fig. 7,

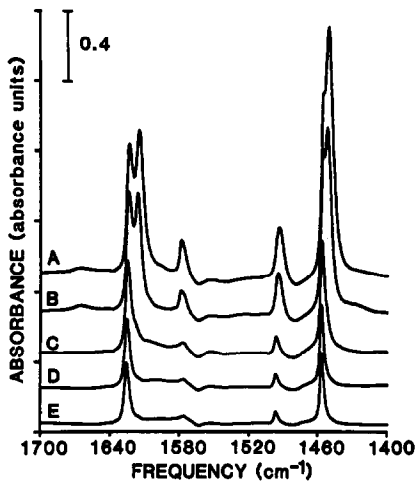

FIG. 7. Infrared spectra of pyridine adsorbed on γ-Al_2O_3 after oxidation in O_2 at 723 K. Evacuation temperature and pressure: (A) 423 K, 7×10^{-4} Torr; (B) 423 K, 2×10^{-4} Torr; (C) 523 K, 1×10^{-4} Torr; (D) 623 K, 9×10^{-5} Torr; (E) 723 K, 8×10^{-5} Torr.

TABLE 5

Infrared Absorption Frequencies (cm^{-1}) for Spectra of Pyridine Adsorbed on γ-Al_2O_3 Shown in Fig. 7

Type	Band	Evacuation treatment: temperature and pressure (Torr)				
		423 K, 7×10^{-4}	423 K, 2×10^{-4}	523 K, 1×10^{-4}	623 K, 9×10^{-5}	723 K, 8×10^{-5}
LPY(I)	19b	1451	1452			
	19a	1493	1494			
	8b	1578	1579			
	8a	1615	1616			
LPY(II)	19b	1455sh	1455	1456	1456	1456
	19a	1493	1494	1496	1496	1496
	8b	1578	1579	1577	1576	1576
	8a	1624	1624	1625	1626	1626

Note. LPY(I) = Lewis pyridine number 1; LPY(II) = Lewis pyridine number 2; sh = shoulder.

for which the frequencies are tabulated in Table 5. Two distinct peaks for both the 8a and 19b bands appear in these spectra. These two bands have been observed previously (e.g. (*18, 19*)). The frequencies of the 8a bands in spectrum A are at 1615 and 1624 cm^{-1}. Note that the low frequency band is the same as that observed on α-Al_2O_3. Desorption of the pyridine at 523 K results in spectrum C in which the lower wavenumber peaks of each pair can no longer be resolved. Evacuation at 723 K (spectrum E) does not remove the high wavenumber peaks, indicating that the pyridine is strongly bonded to these sites. It has often been postulated that these high frequency peaks are due to coordinatively unsaturated Al^{3+} cations in tetrahedral sites. The lower wavenumber band has been assigned to an anion vacancy over a tetrahedral and an octahedral Al cation (*9*). This assignment implies that tetrahedral cations exist on the α-Al_2O_3 surface; however, no peaks are observed at the high wavenumber due to tetrahedral cations. The small peak at 1597 cm^{-1} of α-Al_2O_3 has been previously assigned to unsaturated octahedral cations (*9*). However, one would expect that the band at this low wavenumber to be due to physisorbed pyridinc (c.g., as observed on MgO). Furthermore, while the 1597 cm^{-1} peak is present in spectrum 6A, it disappears in spectrum B, which is for the same evacuation temperature of 423 K but after the pyridine pressure has been reduced from 1×10^{-3} to 2×10^{-4} Torr. A simpler explanation of the IR spectra for pyridine on Al_2O_3 would be that the lower wavenumber peak at 1615 cm^{-1} is a result of octahedral cations only. This would be consistent with the spectra of pyridine on α-Al_2O_3 as well as the large amount of pyridine found adsorbed on α-Al_2O_3 with the gravimetric adsorption measurements. Thus, it is proposed that the high and low wavenumber peaks observed for γ-Al_2O_3 can be assigned to coordinatively unsaturated "tetrahedral and octahedral" cations, respectively.

It has been shown in the literature that one can expect to observe different peaks in the IR of pyridine corresponding to adsorption on different cations. Tret'yakov and Filimonov (*20*), for example, determined the infrared absorption frequency for pyridine adsorbed on a series of oxides. They concluded that the frequency was dependent on the cation, not on its environment. This has been shown to be true for Fe in various phases. The 8a band for pyridine is between 1607 and 1613 cm^{-1} for α-Fe_2O_3 (*21, 22*), γ-Fe_2O_3 (*23*), and FeOOH (*24–26*). In Part I of this series (*4*), a pyridine IR peak due to Fe^{3+} on SiO_2 was found at 1611 cm^{-1}. Hence, one would expect to see a peak near 1611 cm^{-1} for the Fe/Al_2O_3 sample if acid sites associated with Fe^{3+} cations were present on alumina. As seen in Figs. 2A–C and Table 6, this was not observed. Thus, there is no evidence from the infrared data to confirm the addition of new acid sites on the surface of Al_2O_3 upon addition of Fe. However, since the amount of adsorbed pyridine on Al_2O_3 is much higher at the low evacuation temperatures, one may expect the Fe peaks to be obscured by the Al_2O_3 peaks. However, even at the higher evacuation temperatures, where the fraction of sites due to Fe is higher (as observed by the gravimetric adsorption data), no peak attributable to Fe is observed. One

TABLE 6

Infrared Absorption Frequencies (cm^{-1}) for Spectra of Pyridine Adsorbed on 0.6 wt% Fe/γ-Al_2O_3 Shown in Figs. 2A–C

Type	Band	Evacuation treatment: temperature and pressure (Torr)		
		423 K, 9×10^{-4}	423 K, 2×10^{-4}	523 K, 2×10^{-4}
LPY(I)	19b	1451	1452	
	19a	1494	1494	
	8b	1578	1578	
	8a	1616	1616	1616sh
LPY(II)	19b	1455	1455	1456
	19a	1494	1494	1496
	8b	1578	1578	1576
	8a	1624	1624	1625

Note. LPY(I) = Lewis pyridine number 1; LPY(II) = Lewis pyridine number 2; sh = shoulder.

must also remember that while the sample is cooling to room temperature before collection of the spectra readsorption of pyridine may occur on the sample, thereby increasing the amount of adsorption on Al_2O_3. In addition, the evacuation pressures are an order of magnitude higher in the IR cell than in the gravimetric adsorption apparatus (i.e., 10^{-4} versus 10^{-5} Torr, respectively).

Iron Supported on TiO_2

Mössbauer spectroscopy. Oxidation of the 0.6 wt% Fe/TiO_2 sample in O_2 at 723 K gave the spectrum depicted in Fig. 8A, with the parameters summarized in Table 7. The spectrum was fit with a doublet having an isomer shift of 0.33 mm/s and a quadrupole splitting of 1.2 mm/s. Reduction of Fe/TiO_2 in H_2 at 673 K led to the complex spectrum shown in Fig. 8B. It has been fit with four doublets. There is evidence for some residual Fe^{3+}, and hence a weak doublet with the same parameters as in spectrum A has been used in fitting the spectrum. Three doublets were used to fit the Fe^{2+} part of the spectrum. The most intense doublet is similar to the doublets seen on MgO, Al_2O_3, and SiO_2 and has an isomer shift of 1.0 mm/s and a quadrupole splitting of 1.8 mm/s. The peak with the next largest area causes the dip between the two major peaks. This doublet has an isomer shift of 0.85 mm/s and a quadrupole splitting of 0.75 mm/s. This same doublet has been observed on 0.1 wt% TiO_2 by Murrell and Garten (*27*) with an isomer shift of 0.89 mm/s and a quadrupole splitting of 0.58 mm/s. This is also similar to the doublet observed on SiO_2 in Part I of this series (*4*) as well as in previous works (*12, 28–31*). A similar doublet has also been observed on Y-zeolite (*32–34*), L-zeolite (*35*), A-zeolite (*36*), and mordenite (*37*). This doublet has been denoted as an "inner doublet" due to its small isomer

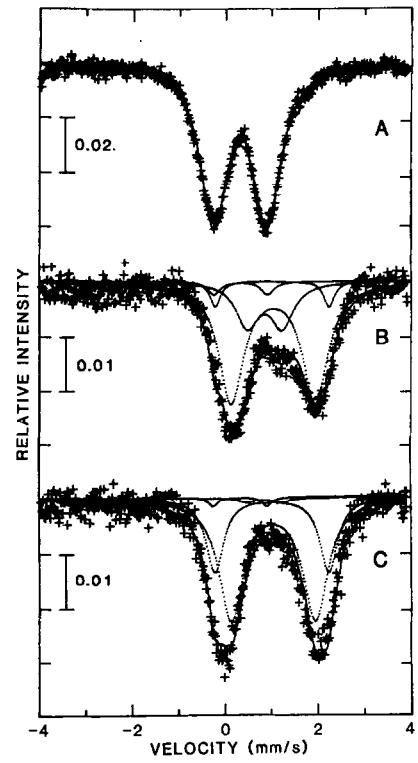

FIG. 8. Room temperature Mössbauer spectra for 0.6 wt% Fe/TiO_2. (A) After oxidation in O_2 at 723 K; (B) after reduction in H_2 at 673 K; (C) after reduction in H_2 at 673 K followed by pyridine adsorption in H_2 at 423 K for 1 h and degassing in flowing H_2 at 423 K for 4 h.

TABLE 7

Mössbauer Parameters for Spectra of 0.6 wt% Fe/TiO_2 Shown in Fig. 8

Species		Treatment: gas and temperature		
		O_2 723 K	H_2 673 K	H_2/pyridine, H_2 423 K
Fe^{3+}				
Isomer shift	0.33 mm/s			
Quadrupole splitting	1.16 mm/s			
Fractional area		1.00	0.04	0.02
Linewidth (mm/s)		0.70	0.34	0.26
Area (pct. * mm/s)		12.41	0.26	0.14
Fe^{2+} inner doublet				
Isomer shift	0.85 mm/s			
Quadrupole splitting	0.75 mm/s			
Fractional area			0.22	0.02
Linewidth (mm/s)			0.60	0.42
Area (pct. * mm/s)			1.46	0.12
Fe^{2+} outer doublet I				
Isomer shift	1.04 mm/s			
Quadrupole splitting	1.82 mm/s			
Fractional area			0.68	0.67
Linewidth (mm/s)			0.65	0.65
Area (pct. * mm/s)			4.46	4.45
Fe^{2+} outer doublet II				
Isomer shift	1.01 mm/s			
Quadrupole splitting	2.46 mm/s			
Fractional area			0.06	0.30
Linewidth (mm/s)			0.28	0.47
Area (pct. * mm/s)			0.40	1.97

shift and quadrupole splitting, and it has been assigned to Fe^{2+} cations held in sites of low coordination on the surface. These cations are capable of adsorbing molecules from the gas phase such as NO, H_2O, and NH_3.

Adsorption of pyridine on the Fe/TiO_2 sample followed by degassing in H_2 at 423 K gave the Mössbauer spectrum shown in Fig. 8C. As can be seen, the inner doublet essentially disappears and the outermost doublet increases in spectral area upon adsorption of pyridine. This outermost doublet has an isomer shift of 1.0 mm/s and a quadrupole splitting of 2.5 mm/s. Because all of the doublets overlap, assignments were not trivial. The Fe^{3+} doublet was constrained to be at the same position as in the fully oxidized sample. Next, the two spectra B and C were subtracted to reveal the changes upon the adsorption of pyridine. The innermost and outermost doublets that changed in area were fixed by this procedure. Next, holding these constant, the spectra were refit to obtain parameters for the outer doublet, or the largest area Fe^{2+} doublet that does not change with the adsorption of pyridine. Once this doublet was fit, all of its parameters were fixed including the dip and width. The innermost and outermost doublets that are perturbed by pyridine were then refit. Finally, after obtaining

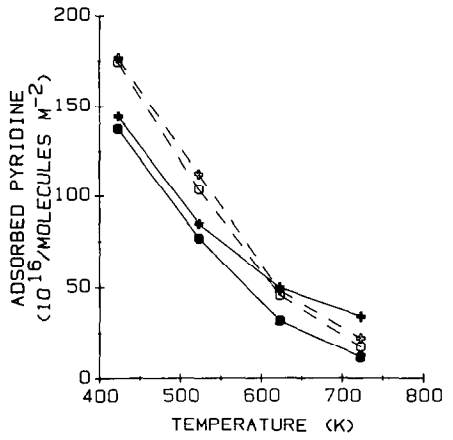

FIG. 9. Gravimetric measurements of pyridine adsorption on 0.6 wt% Fe/TiO_2: (✣) TiO_2 after oxidation in O_2 at 723 K; (○) TiO_2 after reduction in H_2 at 723 K; (✚) Fe/TiO_2 after oxidation in O_2 at 723 K; (●) Fe/TiO_2 after reduction in H_2 at 723 K.

a good fit for the entire spectrum, all three doublets were left unconstrained to obtain the best fit. Desorption of pyridine at 550 K gave a spectrum with a ratio of the inner doublet to the outermost doublet intermediate between the ones with and without pyridine. The original spectrum was obtained after degassing at 673 K. Thus Mössbauer spectroscopy shows evidence for acid sites associated with iron on the surface of TiO_2.

Pyridine adsorption measurements. The results of the gravimetric measurements of pyridine adsorption are shown in Fig. 9. The two upper curves are for TiO_2 alone after oxidation and reduction at 723 K. It is interesting that the reduction of TiO_2 in H_2 at 723 K, which produces Ti^{3+} as evidenced by the intense blue color of the sample as well as complete opacity in the IR, does not affect the pyridine adsorption. This is in contrast with catalytic work in which Ti^{3+}, which makes TiO_2 an *n*-type semiconductor, can act as a base toward probe reactions (*38, 39*). Thus, it can be concluded that, while Ti^{3+} can affect the basic properties of the oxygen anions by being a source of electrons, this does not alter the acidity of the surface. Either the surface cations remain Ti^{4+} after reduction or the same surface concentration of Ti^{3+} exists for the oxidized and reduced samples (since both samples are treated under vacuum for 0.5 h at 723 K prior to pyridine adsorption studies).

Addition of Fe to the sample has a marked effect on the adsorption of pyridine, as shown in Fig. 9. The Fe poisons some of the weaker acid sites in both the oxidized and reduced states. The number of sites corresponds to 30% of the added Fe. The Mössbauer spectra indicate that there are acid sites associated with Fe, corresponding to 20% of the spectral area. Hence, it can be estimated that half of the added Fe cations are selectively adsorbed on the surface of titania, either blocking acid sites or creating new acid sites. This has been observed previously by Murrell and Garten (*27*). Similar behavior was also observed for a sample of Ti dispersed on SiO_2 (*40*). Specifically, Rh added to the surface of Ti/SiO_2 decreased monotonically the number of acid sites that were originally generated by the addition of Ti to SiO_2.

A difference between the oxidized and reduced Fe/TiO_2 samples can be seen in Fig. 9 with respect to the desorption of pyridine at progressively higher temperatures. The reduced sample follows the same curve of adsorption versus evacuation temperature as the TiO_2 blanks. Thus, there is no increase in the strength of the acid sites for Fe^{2+} above that of TiO_2 alone, even though it has been proven by Mössbauer spectroscopy that there are acid sites on Fe^{2+}. The curve for the oxidized Fe/TiO_2 sample, however, crosses the line of the TiO_2 blanks at 623 K. At the 723 K evacuation temperature, there is a larger amount of pyridine adsorbed on Fe/TiO_2 than on the TiO_2 blank. This is evidence that the addition of Fe^{3+} to TiO_2 creates new, stronger acid sites.

Infrared spectra of pyridine adsorbed on TiO_2 and Fe/TiO_2 are shown in Figs. 10A–C and 10D–F, respectively. The corresponding band frequencies are summarized in Table 8. It can be seen that peaks for Lewis acid sites are present. The peak

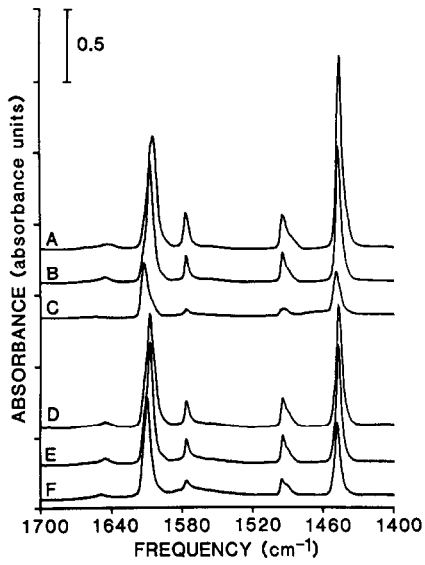

FIG. 10. Infrared spectra of pyridine adsorbed on TiO_2 (A–C) and 0.6 wt% Fe/TiO_2 (D–F) after oxidation in O_2 at 723 K. Evacuation temperature and pressure: (A) 423 K, 1×10^{-3} Torr; (B) 423 K, 2×10^{-4} Torr; (C) 523 K, 2×10^{-4} Torr; (D) 423 K, 7×10^{-4} Torr; (E) 423 K, 2×10^{-4} Torr; (F) 523 K, 1×10^{-4} Torr.

shapes are not symmetrical indicating that there is a distribution of sites, with a major amount being stronger sites that absorb at higher frequencies. In spectra A–C for TiO_2, the 8a peak shifts in an abrupt manner from 1604 to 1607 and 1612 cm^{-1} upon evacuation. This behavior has been assigned previously (*41*) to three distinct types of coordinatively unsaturated Ti cations. The large frequency shift between spectra A and B can be attributed to the loss of physisorbed pyridine. After evacuation at 623 K, the sample became opaque to the IR beam because of the formation of Ti^{3+}, and no pyridine bands could be detected through the sample at this or the 723 K evacuation. There is also a small peak at 1642 cm^{-1}. This has been assigned to a combination mode of the (1 + 6a) vibrations (*41*). This is not part of a Brønsted acid peak because there is no corresponding peak at 1540 cm^{-1}.

The addition of Fe^{3+} to the titania surface does not significantly alter the infrared spectra, as shown in Figs. 10D–F. The major difference is the sharpening of the 8a peak near 1610 cm^{-1}, which then increases the intensity ratio of the 8a to 19b band. Note also that the peak maxima do not shift as much with evacuation. This is a result of the narrower peak. This is consistent with the poisoning of the weak sites by Fe suggested by the gravimetric measurements. It should be remembered that pyridine on Fe^{3+} is expected to give a band at 1611 cm^{-1}, which overlaps with the band for pyridine on TiO_2. However, the sharpening of the bands gives evidence for the effect of Fe^{3+} in changing the acid site strength distribution on TiO_2. Finally, IR studies of pyridine adsorbed on Fe^{2+} cations on titania could not be conducted because reduction of the Fe/TiO_2 sample makes TiO_2 opaque before any pyridine is added, and no pyridine peaks can be observed in the infrared transmission mode.

TABLE 8

Infrared Absorption Frequencies (cm^{-1}) for Spectra of Pyridine Adsorbed on TiO_2 and 0.6 wt% Fe/TiO_2 Shown in Fig. 10

Spectra A–C: TiO_2		Evacuation treatment: temperature and pressure (Torr)		
Type	Band	423 K, 1×10^{-3}	423 K, 2×10^{-4}	523 K, 2×10^{-4}
LPY	19b	1445	1446	1448
	19a	1494	1494	1493
	8b	1576	1576	1576
	8a	1604	1607	1612
Spectra D–E: Fe/TiO_2		423 K, 7×10^{-4}	423 K, 2×10^{-4}	523 K, 1×10^{-4}
Type	Band			
LPY	19b	1447	1447	1448
	19a	1494	1494	1495
	8b	1576	1576	1576
	8a	1608	1608	1610

Note. LPY = Lewis pyridine.

TABLE 9

Metal-to-Oxygen Bond Strengths of the Host Oxides Based on Heats of Formation at 298 K[a]

Oxide	Metal-to-oxygen bond strength (kJ/mol)	
	Reference state: Neutral species	Charged species
MgO	166	660
Al_2O_3	293	1495
TiO_2	314	2040
SiO_2	315	3195

[a] Heats of formation from Ref. (*42*); ionization energies and electron affinities from Ref. (*43*).

DISCUSSION

Single Component Oxides

In this study, comparisons can be made of the acidities of the various oxides because all of the data have been collected under internally consistent conditions. In this respect, it is useful to consider metal–oxygen bond strengths, electronegativity and Pauling's electrostatic bond strength, combined with ideas of coordination and geometry.

The metal-to-oxygen bond strengths for the host oxides used in this study are given in Table 9. These were calculated as the heats per mole of oxygen atoms required to form neutral gaseous metal and oxygen atoms from the oxide. The heat has been divided by the coordination of oxygen to give the strength of each metal-to-oxygen bond. An average oxygen coordination of 3.5 has been used for Al_2O_3. As can be seen, MgO has the lowest metal-to-oxygen bond strength, whereas SiO_2, TiO_2, and Al_2O_3 have considerably higher strengths. However, when an anion is removed from a cation, charged species are created. Hence the bond strength is also given assuming that the oxide is formed from the gaseous metal cations and oxygen anions. In this case the oxide ordering remains the same but there is a larger difference between Al_2O_3, TiO_2, and SiO_2. In the oxide the electrons are not completely removed from the cations so that the reference state is not fully ionized cations or neutrals. The true situation is intermediate between the two cases shown. In both situations the metal-to-oxygen bond strength is ranked in the order of $MgO < Al_2O_3 < TiO_2 < SiO_2$. It should be noted that this same ordering exists if the bond strength is calculated as a weighted average between the above two extreme values, using electronegativity values to estimate the charge of the oxygen anions (*44, 45*).

As is known from the literature, MgO and SiO_2 do not contain acid sites of either the Brønsted or Lewis type. The low Sanderson electronegativity of MgO (3.22) combined with the octahedral coordination of Mg dictates that MgO will be basic. Since the coordination of each magnesium and oxygen atom is six, coordinative unsaturation of the cation by one ligand takes only $\frac{1}{6}$ of the crystal stabilization energy. The low metal-to-oxygen bond strength also leads to a small amount of energy to unsaturate the cation. Hence, the driving force to complete saturation by adsorption of an electron donating molecule is small. The low electronegativity also means that oxygen anions attract negative charge from magnesium cations. The donation of negative charge to an acceptor thus has a large driving force and MgO is basic.

Silica, on the other hand, has a high Sanderson electronegativity (4.14) and lower coordination numbers. The higher electronegativity indicates that silicon cations compete effectively with oxygen anions for negative charge. This leads to covalent bonding. The coordination of four for Si and two for oxygen also indicates that breaking one Si—O bond requires a large amount of energy. A coordinatively unsaturated Si^{4+} cation would thus be in a high energy state, and there would be a large driving force to resaturate the Si^{4+} cations. The driving force is such that coordinatively unsaturated Si^{4+} would readily dissociate an H_2O molecule to form surface hydroxyl groups (*46*). In addition, any oxy-

gen that has had a Si—O bond broken will be missing half of its coordination and will accept a proton from the available H_2O. This proton will be strongly held and thus not be acidic. Thus, acid sites are not generally observed on silica, as was the case in the present study.

Conversely, alumina and titania exhibited large numbers of acid sites in this study. Alumina has a high electronegativity (3.72) but not as high as SiO_2 (4.14). In addition, the crystal structure of γ-Al_2O_3 has Al in both four- and sixfold coordinations, and oxygen has an average coordination between three and four. Breaking one of the six Al—O bonds for an octahedral Al does not take as much energy as for the case of SiO_2. Thus, coordinatively unsaturated Al^{3+} cations can be formed by removing water from the surface at the temperatures used in this work. The breaking of an Al—O bond of a tetrahedral Al requires more energy, but coordinatively unsaturated cations are apparently also produced on the surface. These ideas of strength per bond are reflected in the electrostatic bond strength of Pauling (*6*). Its usefulness is demonstrated in the present study in that the tetrahedral Al cations appear to be stronger acid sites than octahedral Al cations. This is evidenced in the infrared spectroscopy of adsorbed pyridine on α- and γ-Al_2O_3. Interestingly, the numbers of acid sites on α-Al_2O_3 and γ-Al_2O_3 are comparable. Hence, whether the Al cations are tetrahedrally or octahedrally coordinated does not change the number of sites; i.e., only the strength of the acid sites is affected by the coordination.

The electronegativity of titania (3.36) is lower than that of alumina and the coordination of the titanium cations is six. Accordingly, it could be suggested that titania should be less acidic than alumina. However, the coordination of the oxygen anions in titania (i.e., 3) is lower than that in alumina. Furthermore, titania acts as an acid toward catalytic probe reactions, and the isoelectric point of titania in aqueous solution is at slightly lower pH than for alumina (*47*). Thus, titania and alumina may well show similar acidic properties. Indeed, of the oxides investigated in this study, titania showed the greatest number of acid sites per surface area.

In summary, as the electronegativity increases, the covalency of the bonding increases along with the acidic character. The coordination participates in determining the acidic or basic character as well. Lower cation and anion coordinations generally lead to stronger acid sites. The number of acid sites observed by adsorption methods is dependent on the acid strength because only a range of acid strengths are deemed to be acids. With low acid strength, basic probe molecules are not chemisorbed on the surface and no acid sites are measured. As the acid strength increases, more acid sites are measured. Finally, as the acid strength increases further, the number of measured acid sites decreases because only neutralized acid sites are encountered on the surface (e.g., sites that have reacted with water). Thus, the number of acid sites measured goes through a maximum when plotted against the acid strength.

Supported Iron Oxide Samples

The addition of iron to the above oxides adds several complicating factors from an experimental viewpoint which must be addressed before the discussion of the chemical effects. First, it is important whether the dopant cations are on the surface. The added cations may diffuse into the bulk and thus not participate in surface reactions. The added cation may also form a compound with the host oxide, and as such it may participate in establishing the oxygen charge and coordination. This will ultimately affect the way any other foreign cations are bonded to the surface as well as affect the inherent acidity of the oxide. Finally, it must be remembered that if the number of acid sites on the host oxide alone is too high, the effect of adding a small

amount of dopant cannot be measured within experimental error.

The results of the present study can be discussed with these factors in mind. Adding Fe to MgO does not generate new acid sites. The high coordination number of oxygen (i.e., 6) dictates that many iron-to-oxygen bonds are required to provide for charge neutrality of iron. For example, based on the formal charges of two for Mg and O, six Fe—O bonds would be needed to coordinate Fe^{2+}. The full coordination of Fe by oxygen is evidenced by the lack of acid sites. Furthermore, a fraction of the Fe^{2+} diffused into the MgO support, and the Fe^{3+} was present as magnesium ferrite. Another reason for the lack of acidity for Fe/MgO is that the basic character of the oxygen anions may neutralize any acid sites formed.

On alumina, a small number of new acid sites is apparently observed after the addition of Fe. In this case, basic anions are not present to neutralize acid sites. The average coordination of oxygen is between three and four so that the Pauling electrostatic bond strength of each bond is greater than for MgO. Coordinatively unsaturated Fe cations may be expected on the surface without violating charge neutrality. Based on the formal charges, an Fe^{2+} cation needs four Fe—O bonds and Fe^{3+} requires six. However, there is evidence for compound formation which prevents most of the iron from becoming acidic. Formation of the aluminum spinel is facile in that both γ-Al_2O_3 and $FeAl_2O_4$ have the same structure. There were, however, some Fe cations on the surface. Room temperature oxidation completely oxidized a reduced sample. In addition, Mössbauer spectra taken but not explicitly reported indicated that 75% of the iron was perturbed by reaction with 1 atm of NO.

New acid sites are formed upon addition of iron to titania. In addition, the number of acid sites on TiO_2 decreases. Thus, the oxygen anions associated with Fe apparently coordinate with Ti. The iron is held on titania in sites of low coordination, as observed with Mössbauer spectroscopy. The coordination of the oxygen anions in titania is three, and this makes it possible to hold Fe^{2+} on the surface with enough bonds to provide for charge neutrality, yet leave it coordinatively unsaturated. Using Pauling's electrostatic bonding rules, one needs three Fe—O bonds for Fe^{2+} and 4.5 bonds for Fe^{3+}. Iron cations of low coordination chemisorb pyridine and hence are acidic. Iron 3+ has a higher electronegativity than Ti^{4+} and hence the strength of the acid sites is higher for Fe^{3+} than for Ti^{4+}. This was observed with the gravimetric adsorption measurements. Iron 2+, on the other hand, is not much different from TiO_2 in electronegativity. Therefore, no enhancement of the acid strength was observed.

Finally, the number of acid sites has been shown to be greatly increased by adding Fe to SiO_2 (*4*). Experimentally this is an ideal system because the absence of acidity on SiO_2 allows for unequivocal measurements of the acidity on Fe. The Si^{4+} cations are small and the structure of silica is such that Fe will not dissolve into the bulk. There is formation of Fe/SiO_2 complexes only on the surface. The oxygen coordination of two in SiO_2 leads to the prediction that SiO_2 may be capable of holding Fe^{2+} cations in sites of low coordination, thus leaving them coordinatively unsaturated. Indeed, Mössbauer spectroscopy shows evidence that 70% of the Fe cations are in sites of low coordination. In a formal sense, only two bonds are required to hold an Fe^{2+} cation in that oxidation state and only three are required for an Fe^{3+} cation.

Model of Lewis Acidity

It should be noted that Brønsted acid sites were not observed on this series of samples prepared by depositing iron on MgO, Al_2O_3, TiO_2, and SiO_2. The acid sites were all of the Lewis type and their existence can be explained in terms of unsaturated cations in various structures. This is in contrast to the Tanabe model (*5*) which

predicts Brønsted acidity for Fe^{2+}/Al_2O_3, Fe^{2+}/TiO_2, Fe^{2+}/SiO_2, Fe^{3+}/TiO_2, and Fe^{3+}/SiO_2. It predicts Lewis acidity for Fe^{3+}/MgO and no acidity for Fe^{2+}/MgO and Fe^{3+}/Al_2O_3. Therefore, the Tanabe model correctly predicts the acidity for only one out of eight systems and this is for Fe^{2+}/MgO in which no acidity is predicted or observed. It should be noted that the Tanabe model was originally proposed for mixed metal oxides, and we have attempted here to extend this model to supported metal oxides.

The model proposed here for acidity is somewhat like the Tanabe model in form but not in conclusion. The important parameter in the generation of new acid sites on the surface of mixed oxides is the structure of sites. Lewis acidity is described in terms of coordinatively unsaturated cations, as shown by Mössbauer spectroscopy for Fe on both SiO_2 and TiO_2. Hence, to have Lewis acidity for a binary oxide one must have coordinatively unsaturated cations on the surface. However, this is a necessary not a sufficient condition. The character of the host oxide must be acidic or at least not strongly basic. For example, unsaturated Mg cations may well be present on MgO; however, no acid sites are observed. Yet, when Mg is placed on SiO_2, the coordinatively unsaturated cations are acidic (*7, 48*). Further evidence that a surface free of strong basic sites is required is the fact that preadsorption of CO_2 on ZnO increases the strength of the acid sites (*49*).

In short, a coordinatively unsaturated cation free from strong basic oxygen anions is the model of Lewis acid sites proposed. On acidic surfaces this is favored by doping a cation that cannot easily form a solid solution or a crystalline mixed oxide. The mixture should be such that the dopant cation will remain on the surface yet be bonded to the host oxide sufficiently strongly that it does not sinter into particles of its own oxide. Pauling's electrostatic bonding rules can be used as a guide in predicting the behavior. If the required number of cation-to-oxygen bonds to provide for charge neutrality of the dopant cation is less than or equal to four, one apparently has a good chance of forming unsaturated cations. As the predicted coordination number decreases, the probability of forming acid sites becomes greater.

The strength of the Lewis acid sites has not been addressed in the present paper; i.e., this model only predicts the existence of Lewis acids. A prediction of Brønsted acidity is also not covered in these predictions. It will be shown elsewhere (*7*) that the Lewis acid strength can be correlated with electronegativity for a given geometry. The existence of Brønsted acidity will be explained in terms of a special bonding configuration which gives this type of acid site.

CONCLUSIONS

Pyridine adsorption was used to identify Lewis acid sites on the surface of Al_2O_3 and TiO_2. No acid sites were observed for MgO and SiO_2 (*4*). These data were explained in terms of coordination, metal–oxygen bond strength and electronegativity.

The addition of Fe to the surface of TiO_2 and SiO_2 altered the acidic properties. New acid sites as a result of the added Fe were observed in conjunction with the appearance of low coordination Fe cations on the surface. These coordinatively unsaturated iron cations were proven by Mössbauer spectroscopy to be acidic. There was no evidence for coordinatively unsaturated Fe on MgO or Al_2O_3 and little or no new acidity was observed for these systems upon addition of iron.

The acidity of binary oxides formed by doping one oxide onto another has been modeled based on the structural environment of the acid sites. A model of Lewis acidity is proposed that gives a criterion for the existence of coordinatively unsaturated cations on the surface. One simply calculates the number of bonds required for the dopant cation to be electrically neutral in the host oxide. If this number is less than or equal to four, Lewis acidity is predicted to

be observed for the dopant cations that are on the surface of the oxide. This model includes the predictions of the Tanabe model because both models utilize similar assumptions regarding the anion and cation coordinations.

ACKNOWLEDGMENTS

We would like to thank American Cyanamid for providing us with the alumina. We also would like to thank Amoco for providing one of us (G.C.) with a fellowship during the course of this study. In addition, support for this work was provided by the Office of Basic Energy Sciences of the Department of Energy (DE-FG02-84ER13183), and it is gratefully acknowledged.

REFERENCES

1. Jin, T., Hattori, H., and Tanabe, K., *Bull. Chem. Soc. Japan* **55,** 2279 (1982).
2. Tanabe, K., Itoh, M., Morishige, K., and Hattori, H., *in* "Preparation of Catalysts" (B. Delmon, P. A. Jacobs, and G. Poncelet, Eds.), p. 65. Elsevier, Amsterdam, 1976.
3. Shibata, K., Kiyoura, T., Kitagawa, J., Sumiyoshi, T., and Tanabe, K., *Bull. Chem. Soc. Japan* **46,** 2985 (1973).
4. Connell, G., and Dumesic, J. A., *J. Catal.* **101,** 103 (1986).
5. Tanabe, K., Sumiyoshi, T., Shibata, K., Kiyoura, T., and Kitagawa, J., *Bull. Chem. Soc. Japan* **47,** 1064 (1974).
6. Pauling, L., "The Nature of the Chemical Bond," 3rd ed., p. 547. Cornell Univ. Press, Ithaca, N.Y., 1960.
7. Connell, G., and Dumesic, J. A., submitted to J. Catal.
8. Koubowetz, F., and Noller, H., *Z. Naturforsch, B: Anorg. Chem., Org. Chem.* **32,** 37 (1977).
9. Morterra, C., Coluccia, S., Chiorino, A., and Boccuzzi, F., *J. Catal.* **54,** 348 (1978).
10. Santos, J., Phillips, J., and Dumesic, J. A., *J. Catal.* **81,** 147 (1983).
11. Boudart, M., Delbouille, A., Dumesic, J. A., Khammouma, S., and Topsøe, H., *J. Catal.* **37,** 486 (1975).
12. Rethwisch, D. G., and Dumesic, J. A., *J. Phys. Chem.* **90,** 1863 (1986).
13. Pilipenko, V. I., and Popovskii, V. V., *React. Kinet. Catal. Lett.* **6,** 23 (1977).
14. Borghard, W. S., and Boudart, M., *J. Catal.* **80,** 194 (1983).
15. Sushumna, I., and Ruckenstein, E., *J. Catal.* **90,** 241 (1984).
16. Rossiter, M. J., *J. Phys. Chem. Solids* **26,** 775 (1965).
17. Rethwisch, D. G., and Dumesic, J. A., *J. Phys. Chem.* **90,** 1625 (1986).
18. Knözinger, H., *in* "Advances in Catalysis" (D. D. Eley, H. Pines, and P. B. Weisz, Eds.), Vol. 25, p. 184. Academic Press, New York, 1977.
19. Morterra, C., Chiorino, A., Ghiotti, G., and Garrone, E., *J. Chem. Soc. Faraday Trans. 1* **75,** 271 (1979).
20. Tret'yakov, N. E., and Filimonov, V. N., *Kinet. Catal.* **14,** 700 (1973).
21. Rochester, C. H., and Topham, S. A., *J. Chem. Soc. Faraday Trans. 1* **75,** 1259 (1979).
22. Busca, G., and Lorenzelli, V., *Mater. Chem.* **6,** 175 (1981).
23. Harrouche, N., Batis, H., and Ghorbel, A., *J. Chim. Phys.* **81,** 277 (1984).
24. Rochester, C. H., and Topham, S. A., *J. Chem. Soc. Faraday Trans. 1* **75,** 872 (1979).
25. Parfitt, R. L., Russell, J. D., and Farmer, V. C., *J. Chem. Soc. Faraday Trans. 1* **72,** 1082 (1976).
26. Morterra, C., Mirra, C., and Borello, E., *Mater. Chem. Phys.* **10,** 139 (1984).
27. Murrell, L. L., and Garten, R. L., *Appl. Surf. Sci.* **19,** 218 (1984).
28. Yuen, S., Chen, Y., Kubsh, J. E., Dumesic, J. A., Topsøe, N., and Topsøe, H., *J. Phys. Chem.* **86,** 3022 (1982).
29. Hobson, M. C., Jr., and Gager, H. M., *J. Colloid Interface Sci.* **34,** 357 (1970).
30. Blomquist, J., Csillag, S., Moberg, L. C., Larsson, R., and Rebenstorf, B., *Acta Chem. Scand. Ser. A* **33,** 515 (1979).
31. Arnold, D., and Hartmut, H., *Wiss. Z.-Friedrich-Schiller-Univ. Jena, Math.-Naturwiss. Reihe* **25,** 843 (1976).
32. Segawa, K-I., Chen, Y., Kubsh, J. E., Delgass, W. N., Dumesic, J. A., and Hall, W. K., *J. Catal.* **76,** 112 (1982).
33. Garten, R. L., Delgass, W. N., and Boudart, M., *J. Catal.* **18,** 90 (1970).
34. Delgass, W. N., Garten, R. L., and Boudart, M., *J. Phys. Chem.* **73,** 2970 (1969).
35. Fitch, F. R., and Rees, L. V. C., *Zeolites* **2,** 33 (1982).
36. Dickson, B. L., and Rees, L. V. C., *J. Chem. Soc. Faraday Trans. 1* **70,** 2038 (1974).
37. Garten, R. L., Gallard-Nechtschein, J., and Boudart, M., *Ind. Eng. Chem. Fundam.* **12,** 299 (1973).
38. Hattori, H., Itoh, M., and Tanabe, K., *J. Catal.* **38,** 172 (1975).
39. Hattori, H., Itoh, M., and Tanabe, K., *J. Catal.* **41,** 46 (1976).
40. Murrell, L. L., and Yates, D. J. C., *in* "Proceedings, 7th International Congress on Catalysis, Tokyo, 1980" (T. Seiyama and K. Tanabe, Eds.), Part B, p. 1470. Elsevier, Amsterdam, 1981.
41. Morterra, C., Ghiotti, G., and Garrone, E., *J. Chem. Soc. Faraday Trans. 1* **76,** 2102 (1980).

42. Stull, D. R., and Prophet, H., Eds., "JANAF Thermochemical Tables," 2nd ed., NSRDS-NBS 37, 1971, and supplement, 1974.

43. Huheey, J. E., "Inorganic Chemistry, Principles of Structure and Reactivity," 2nd ed. Harper & Row, New York, 1978.

44. Sanderson, R. T., "Inorganic Chemistry." Reinhold, New York, 1967.

45. Sanderson, R. T., "Chemical Bonds and Bond Energy." Academic Press, New York, 1971.

46. Morrow, B. A., and Cody, I. A., *J. Phys. Chem.* **80,** 1995 (1976).

47. Parks, G. A., *Chem. Rev.* **65,** 177 (1965).

48. Kermarec, M., Briend-Faure, M., and Delafosse, D., *J. Chem. Soc. Faraday Trans. 1* **70,** 2180 (1974).

49. Lavalley, J. C., Saussey, J., and Bovet, C., *J. Mol. Struct.* **80,** 191 (1982).